ChemComm

Check for updates

A chiral two-dimensional perovskite-like lead-free bismuth(III) iodide hybrid with high phase transition temperature†

Hang Peng,‡ Qin Liu,‡ Yan-Zi Lu,‡ Shu-Jing Yang, Jun-Chao Qi, Xiao-Gang Chen 🅳 * and Wei-Qiang Liao 🅳 *

Bismuth(III) iodide perovskites have attracted great attention as lead-free hybrid semiconductors, but they mainly show zero- and one-dimensional structures. Herein, we report the first two-dimensional chiral perovskite-like bismuth(III) iodide hybrid [(S)-3-aminopyrrolidinium I]$_2$Bi$_{2/3}$I$_4$ (1) with a high phase transition temperature of 408.8 K, higher than most of the reported chiral lead-free hybrid semiconductors.

Perovskite materials exhibit numerous fascinating physical properties, such as exotic magnetism, superconductivity, photoelectricity, ferroelectricity, and even multiferroicity.[1-4] Among them, organic–inorganic hybrid perovskites (OIHPs) are a class of important functional materials with perovskite or perovskite-like structures formed by self-assembly of organic cations and an inorganic framework.[5,6] Their structural diversity, mechanical flexibility, ease of fabrication, and other advantages make them show exciting prospects in the field of optoelectronics and photovoltaic applications.[7-11] In recent years, lead-based hybrid perovskites represented by CH$_3$NH$_3$PbI$_3$ have achieved promising results in the field of high-performance optoelectronic and photovoltaic devices including photodetectors, solar cells, and light emitting diodes (LEDs).[12-17] Nevertheless, the presence of highly toxic lead in the lead halide OIHPs may slow or even hinder the pace of their wide-scale application. Therefore, great progress has been made in the development of lead-free halide OIHPs and their derivatives.[18-23]

Structurally, lead-based iodide hybrid perovskites are characterized by a significant diversity of the anionic structures, from zero-dimensional (0D) isolated, one-dimensional (1D) chain, two-dimensional (2D) layered, or even three-dimensional (3D)

framework.[5] As an important branch, low-dimensional 2D layered perovskites have good long-term phase stability in the air, and without the limitation of interlayer cation length, which provides a broader platform for achieving tunable optoelectronic materials, especially ferroelectrics.[5] Bismuth(III)-based hybrid perovskites, as potentially low toxicity alternatives to lead-based perovskites, have the same 6S^{2}6P^0 electronic configuration as that of lead. However, bismuth(III)-based iodide hybrid perovskites tend to form low-dimensional 0D and 1D perovskite or perovskite-like structures.[24,25] To date, only two cases of bismuth(III)-based iodide perovskite have been reported with a 2D structure, namely (H$_2$AEQT)Bi$_{2/3}$I$_4$ and [(F-PEA)$_3$BiI$_6$].[26,27] In recent years, chiral hybrid semiconductors, including perovskite ones, have gained immense interest owing to their attractive chiral photoelectric properties, and exhibit some fascinating physical properties, such as 2D ferroelectric semiconductors [(R and S)-N-(1-phenylethyl)ethane-1,2-diaminium]PbI$_4$, 1D bismuth halides (R/S-α-methylbenzylammonium)BiI$_4$ with strong second- and third-harmonic generation.[28-34] And as far as we know, the study of chiral 2D bismuth(III)-based iodide perovskites is still scarce.

Phase transition materials are those for which physical properties such as the dielectric, magnetic, second harmonic generation (SHG), and other responses can be reversibly converted under external stimuli (temperature, light, and electric fields), allowing their potential application in information storage, intelligent switches, sensors, and other fields.[35,36] Benefiting from the structural rigidity of the inorganic framework and the flexibility of the organic cations, OIHPs are prone to undergoing ordered-disordered motion, resulting in a structural phase transition, and thus accompanied by interesting physical properties.[37-39] Jakubas and his coworkers have carried out a series of studies on bismuth(III)-based halide hybrid phase transition materials, such as 0D bismuth(III)-iodine hybrid ferroelastic [C$_3$N$_2$H$_5$]$_3$Bi$_2$I$_9$, and 1D bismuth(III)-bromide hybrid ferroelectric (C$_2$H$_5$NH$_3$)$_2$[BiBr$_5$].[24,40-43] The phase transition temperature (T$_c$) is an important key parameter for the application of

Ordered Matter Science Research Center, Nanchang University, Nanchang 330031, People's Republic of China. E-mail: chenxg@ncu.edu.cn, liaowq@ncu.edu.cn
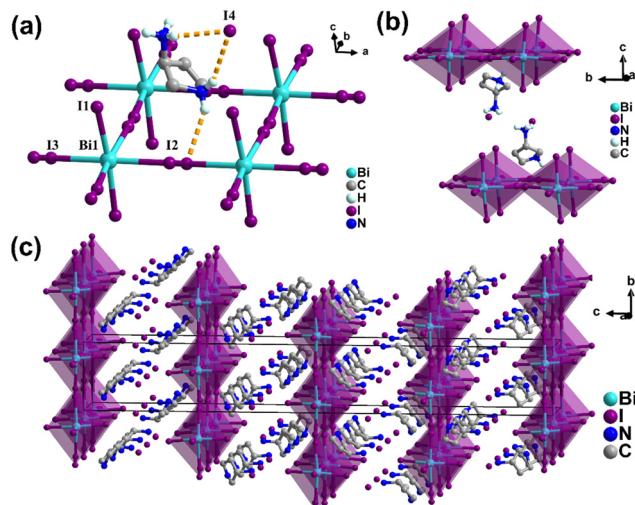
Fig. 1 Crystal structures of **1**. The structural unit (a) and packing view (b) and (c) at 293 K. Some hydrogen atoms are omitted for clarity, and the yellow dotted lines represent hydrogen bonds.

Fig. 2 UV-vis absorption spectra of **1**. The inset shows the *Tauc* plot for determining the optical bandgap and the black–red crystals.

phase transition materials. But unfortunately, up to now, the overwhelming majority of chiral lead-free semiconductor phase transition materials have a relatively low T_c.[24,44–46] In this context, it is important to explore chiral lead-free semiconductors with high T_c for practical applications.

In this work, we used S-3-aminopyrrolidinium dihydroiodate and bismuth(III) iodide to assemble a 2D hybrid perovskite of **1**. The phase purity of **1** was verified by powder X-ray diffraction (PXRD) (Fig. S1, ESI†). The crystal structures of **1** were determined by carrying out single-crystal X-ray diffraction experiments. **1** crystallizes in the tetragonal crystal system with the chiral space group of $P4_12_12$ at 293 K (Table S1, ESI†). The basic unit of **1** consists of two independent S-3-aminopyrrolidinium cations, two isolated I^- anions, and one $[Bi_{2/3}I_4]^{2-}$ anion (Fig. 1). The typical 2D layer perovskite architecture of infinite $[Bi_{2/3}I_4]_n^{2-}$ layers was constructed by corner-sharing BiI_6 octahedra and 1/3 of the vacancy on the metal site, which is the same as the 2D framework of $(H_2AEQT)Bi_{2/3}I_4$ reported by Mitzi *et al.*[26] Each central Bi atom is linked with six I atoms to form a slightly twisted octahedron. The ranges of Bi–I bond lengths and *cis* I–Bi–I bond angles are 3.0330(16)–3.091(3) Å and 83.57(9)–100.16(10)° (Tables S2 and S3, ESI†). Structurally, the S-3-aminopyrrolidinium cations are orientationally ordered. In contrast, for the inorganic framework, both bridging iodides, I(2) and I(3), are refined as disordered, with occupancy fixed at 0.5. The protonated S-3-aminopyrrolidinium cations are linked with the inorganic $[Bi_{2/3}I_4]_n^{2-}$ layers and the isolated I^- anions *via* N–H···I hydrogen bonding interactions (Fig. S2 and S3, ESI†).

The ultraviolet-visible (UV-vis) absorption spectrum was measured to get the optical properties. The solid-state ultraviolet-visible (UV-vis) diffuse reflectance spectrum of **1** is tested to obtain the optical band gap. As described in Fig. 2, the result shows that the absorption edge of **1** is 800 nm, which conforms to the characteristic of dark-red crystals. The optical bandgap value (E_g) of **1** is experimentally determined to be
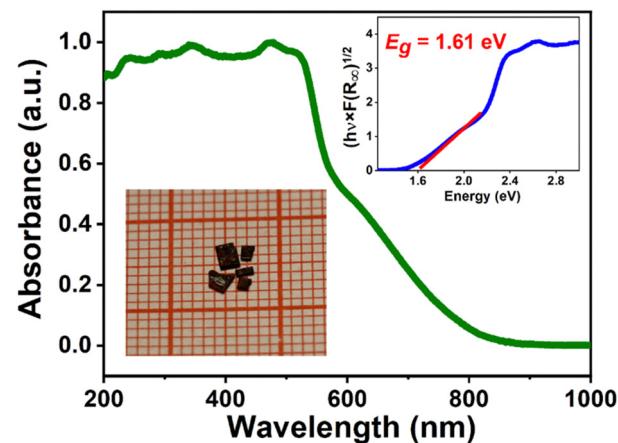
1.61 eV, based on the *Tauc* equation, $(hv \cdot F(R_\infty))^{1/2} = A(hv - E_g)$, where h is Planck's constant, v is the frequency of vibration, $F(R_\infty)$ represents the Kubelka–Munk function, and A is related to the proportional constant, which is smaller than that of $(CH_3NH_3)_3(Bi_2I_9)$ (~ 1.94 eV).[47] This makes **1** have potential applications in narrow bandgap semiconductor-based devices. We carried out circular dichroism (CD) measurements on the single-crystalline powder embedded KBr pellets to study the optical properties. In the spectrum, there are some distinct CD signal peaks, confirming the chirality of **1** (Fig. S4, ESI†).

The phase transition behavior can be directly detected through differential scanning calorimetry (DSC) measurements. As shown in Fig. 3a, the DSC curves of **1** display a pair of reversible abnormal peaks at 408.8/386.4 K in the heating–cooling run. It is worth noting that the T_c of **1** is higher than those of most reported chiral lead-free hybrid semiconductors, such as [(R)-3-hydroxy-pyrrolidinium]$_2$SbBr$_5$ (235/271 K),[44] [(R)-3-hydroxy-pyrrolidinium]$_5$Sb$_4$Br$_{17}$ (315 K),[44] [(R)-3-hydroxyquinuclidinium]$_2$SnCl$_6$ (330 K),[45] and [R-3-hydroxylpiperidinium]$_2$SbCl$_5$ (341 K),[46] and is also outstanding in comparison to those of lead-free hybrid semiconductors.[24] Meanwhile, the phase transition process is often accompanied by dielectric anomalies. We investigated the dielectric response *versus* temperature, which is further strong evidence for phase transitions. As shown in Fig. 3b, we recorded the real part (ε') of the dielectric constant in the range of 320–440 K at a frequency of 1 MHz. When the temperature changes from 320 K to 380 K, the ε' slowly increases from 18.4 to 23.5.
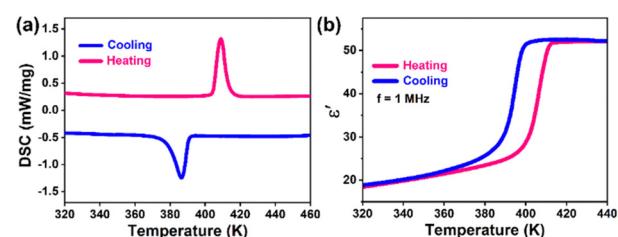
Fig. 3 (a) DSC curves in a heating–cooling cycle. (b) Temperature-dependent dielectric (ε') of **1**.

(a)

(b)
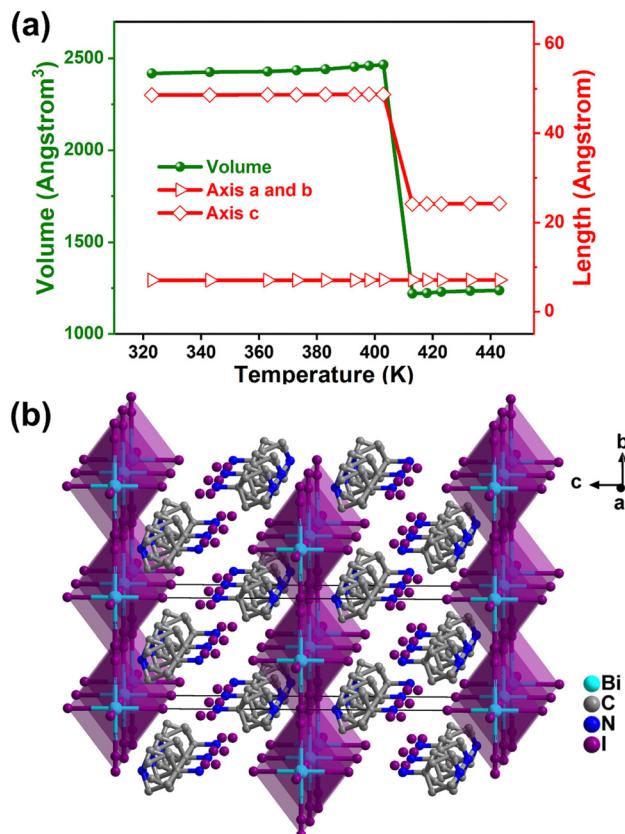
Fig. 4 Temperature dependence of unit-cell parameters (a) and packing view (b) of 1 at 420 K. Hydrogen atoms are omitted for clarity.

As the temperature reaches near T_c, the ε' rises rapidly to 52. As the sample continues to be heated, the value of ε' is almost stable around 52. During the cooling process, there is a dielectric curve similar to the heating process and that has a thermal hysteresis of about 15 K, which is in good agreement with the DSC results. Obviously, the step-like dielectric anomaly of 1 indicates the switchable dielectric characteristics between the high dielectric state and the low dielectric state. The dielectric switching contrast between the high dielectric and low dielectric states of $[(S)$-3-aminopyrrolidinium I]$_2$Bi$_{2/3}$I$_4$ was about 2.21.

Then, we determined the high-temperature crystal structure of 1 above T_c to help reveal the mechanism of the phase transition. As shown in Fig. 4a, with the temperature increasing, the lattice constant of the crystallographic a and b-axis remains almost unchanged, while the length of the c axis in the high-temperature phase (HTP) is approximately half that of the low-temperature phase (LTP), thus resulting in half the volume. At 420 K, 1 still crystallizes in the 422 point group while with a different chiral space group I422. Compared with the structure at 293 K, the main difference lies in the highly disordered S-3-aminopyrrolidinium cations and the disappearance of octahedral distortion (Fig. 4b and Fig. S5, ESI†). Furthermore, variable temperature powder X-ray diffraction (PXRD) measurements have also been taken to probe the phase transition in 1 (Fig. S6, ESI†). The variation in peak number around T_c proved the phase transition of 1. When the temperature was cooled to

293 K, the PXRD pattern was in accordance with the simulated one at 293 K again, indicating its thermal stability and reversibility.

We all know that the inherent stability of materials to heat and humidity is critical for their commercial applications. Bismuth(III)-based materials generally show better stability than CH$_3$NH$_3$PbI$_3$. For example, MA$_3$Bi$_2$I$_9$ film remains stable in the air for more than 25 days, while MAPbI$_3$ film degrades to lead iodide after 25 days exposing to the same ambient air.[48] To study the moisture stability of 1, we exposed the powder sample to ambient air for over one year and recorded its powder X-ray diffraction patterns after six months and one year, respectively. As shown in Fig. S7 (ESI†), the two PXRD patterns are almost the same, and are in good agreement with the freshly-prepared sample one, indicating its excellent moisture stability. In addition, the thermogravimetric analysis (TGA) measurements revealed that 1 is thermally stable up to 520 K without decomposition (Fig. S8, ESI†).

In summary, we synthesized a novel chiral lead-free 2D perovskite-like bismuth(III) iodide hybrid $[(S)$-3-aminopyrrolidinium I]$_2$Bi$_{2/3}$I$_4$. It undergoes a phase transition at around 408.8 K, which is higher than that of most chiral lead-free halide semiconductors including perovskite ones. Simultaneously, 1 shows prominent dielectric switching characteristics between low and high dielectric states around T_c. It is noteworthy to mention that the absorption edge of 1 can reach 800 nm, corresponding to a narrow bandgap. This work enriches the family of 2D lead-free hybrid perovskites and should shed light on the exploration of superior ones.

Conflicts of interest

There are no conflicts to declare.

Notes and references

1 K. I. Kobayashi, T. Kimura, H. Sawada, K. Terakura and Y. Tokura, *Nature*, 1998, **395**, 677–680.
2 T. He, Q. Huang, A. P. Ramirez, Y. Wang, K. A. Regan, N. Rogado, M. A. Hayward, M. K. Haas, J. S. Slusky, K. Inumara, H. W. Zandbergen, N. P. Ong and R. J. Cava, *Nature*, 2001, **411**, 54–56.
3 J. F. Scott, *Science*, 2007, **315**, 954–959.
4 Y. Maeno, H. Hashimoto, K. Yoshida, S. Nishizaki, T. Fujita, J. G. Bednorz and F. Lichtenberg, *Nature*, 1994, **372**, 532–534.
5 B. Saparov and D. B. Mitzi, *Chem. Rev.*, 2016, **116**, 4558–4596.
6 W. Li, Z. Wang, F. Deschler, S. Gao, R. H. Friend and A. K. Cheetham, *Nat. Rev. Mater.*, 2017, **2**, 16099.
7 G. Hodes, *Science*, 2013, **342**, 317–318.
8 W.-J. Xu, P.-F. Li, Y.-Y. Tang, W.-X. Zhang, R.-G. Xiong and X.-M. Chen, *J. Am. Chem. Soc.*, 2017, **139**, 6369–6375.
9 Y.-M. You, W.-Q. Liao, D. Zhao, H.-Y. Ye, Y. Zhang, Q. Zhou, X. Niu, J. Wang, P.-F. Li, D.-W. Fu, Z. Wang, S. Gao, K. Yang, J.-M. Liu, J. Li, Y. Yan and R.-G. Xiong, *Science*, 2017, **357**, 306–309.
10 J. S. Manser, J. A. Christians and P. V. Kamat, *Chem. Rev.*, 2016, **116**, 12956–13008.
11 Y. Peng, X. Liu, L. Li, Y. Yao, H. Ye, X. Shang, X. Chen and J. Luo, *J. Am. Chem. Soc.*, 2021, **143**, 14077–14082.
12 Y. Hu, F. Florio, Z. Chen, W. A. Phelan, M. A. Siegler, Z. Zhou, Y. Guo, R. Hawks, J. Jiang, J. Feng, L. Zhang, B. Wang, Y. Wang, D. Gall, E. F. Palermo, Z. Lu, X. Sun, T.-M. Lu, H. Zhou, Y. Ren, E. Wertz, R. Sundararaman and J. Shi, *Sci. Adv.*, 2020, **6**, eaay4213.

13 I. H. Park, Q. N. Zhang, K. C. Kwon, Z. Y. Zhu, W. Yu, K. Leng, D. Giovanni, H. S. Choi, I. Abdelwahab, Q. H. Xu, T. C. Sum and K. P. Loh, *J. Am. Chem. Soc.*, 2019, **141**, 15972–15976.

14 H. Y. Zhang, X. J. Song, X. G. Chen, Z. X. Zhang, Y. M. You, Y. Y. Tang and R. G. Xiong, *J. Am. Chem. Soc.*, 2020, **142**, 4925–4931.

15 M. Li, Y. Xu, S. Han, J. Xu, Z. Xie, Y. Liu, Z. Xu, M. Hong, J. Luo and Z. Sun, *Adv. Mater.*, 2020, **32**, 2002972.

16 M. K. Jana, R. Y. Song, H. L. Liu, D. R. Khanal, S. M. Janke, R. D. Zhao, C. Liu, Z. V. Vardeny, V. Blum and D. B. Mitzi, *Nat. Commun.*, 2020, **11**, 4699.

17 G. Long, C. Jiang, R. Sabatini, Z.-Y. Yang, M.-Y. Wei, L.-N. Quan, Q.-M. Liang, A. Rasmita, M. Askerka, G. Walters, X.-W. Gong, J. Xing, X.-L. Wen, R. Quintero-Bermudez, H.-F. Yuan, G.-C. Xing, X. R. Wang, D.-T. Song, O. Voznyy, M.-T. Zhang, S. Hoogland, W.-B. Gao, Q.-H. Xiong and E. H. Sargent, *Nat. Photon.*, 2018, **12**, 528–533.

18 H.-Y. Zhang and R.-G. Xiong, *Chem. Commun.*, 2023, **59**, 920–923.

19 H. Lu, C. Xiao, R. Song, T. Li, A. E. Maughan, A. Levin, R. Brunecky, J. J. Berry, D. B. Mitzi, V. Blum and M. C. Beard, *J. Am. Chem. Soc.*, 2020, **142**, 13030–13040.

20 W. Zhang, M. Hong and J. Luo, *J. Am. Chem. Soc.*, 2021, **143**, 16758–16767.

21 Q. Jia, T. Shao, L. Tong, C. Su, D. Fu and H. Lu, *Chin. Chem. Lett.*, 2023, **34**, 107539.

22 X.-G. Chen, Z.-X. Zhang, Y.-L. Zeng, S.-Y. Tang and R.-G. Xiong, *Chem. Commun.*, 2022, **58**, 3059–3062.

23 Z. Xiao, Z. Song and Y. Yan, *Adv. Mater.*, 2019, **31**, 1803792.

24 R. Jakubas, M. Rok, K. Mencel, G. Bator and A. Piecha-Bisiorek, *Inorg. Chem. Front.*, 2020, **7**, 2107–2128.

25 S. A. Adonin, M. N. Sokolov and V. P. Fedin, *Coord. Chem. Rev.*, 2016, **312**, 1–21.

26 D. B. Mitzi, *Inorg. Chem.*, 2000, **39**, 6107–6113.

27 M. Li, H. Li, W. Li, B. Li, T. Lu, X. Feng, C. Guo, H. Zhang, H. Wei and B. Yang, *Adv. Mater.*, 2022, **34**, 2108020.

28 R. Naaman, Y. Paltiel and D. H. Waldeck, *Nat. Rev. Chem.*, 2019, **3**, 250–260.

29 H. Lu, Z. V. Vardeny and M. C. Beard, *Nat. Rev. Chem.*, 2022, **6**, 470–485.

30 Y.-L. Zeng, X.-Q. Huang, C.-R. Huang, H. Zhang, F. Wang and Z.-X. Wang, *Angew. Chem., Int. Ed.*, 2021, **60**, 10730–10735.

31 S. Liu, M. W. Heindl, N. Fehn, S. Caicedo-Davila, L. Eyre, S. M. Kronawitter, J. Zerhoch, S. Bodnar, A. Shcherbakov, A. Stadlbauer, G. Kieslich, I. D. Sharp, D. A. Egger, A. Kartouzian and F. Deschler, *J. Am. Chem. Soc.*, 2022, **144**, 14079–14089.

32 L. Yao, Z. Zeng, C. Cai, P. Xu, H. Gu, L. Gao, J. Han, X. Zhang, X. Wang, X. Wang, A. Pan, J. Wang, W. Liang, S. Liu, C. Chen and J. Tang, *J. Am. Chem. Soc.*, 2021, **143**, 16095–16104.

33 L. Zhao, X. Han, Y. Zheng, M.-H. Yu and J. Xu, *Adv. Photon. Res.*, 2021, **2**, 2100056.

34 Z. Yu, S. Cao, Y. Zhao, Y. Guo, M. Dong, J. Fu, J. Zhao, J. Yang, L. Jiang and Y. Wu, *ACS Appl. Mater. Interfaces*, 2022, **14**, 39451–39458.

35 M. Wuttig and N. Yamada, *Nat. Mater.*, 2007, **6**, 824–832.

36 M. Salinga and M. Wuttig, *Science*, 2011, **332**, 543–544.

37 M. Yang, H. Cheng, Y. Xu, M. Li and Y. Ai, *Chin. Chem. Lett.*, 2022, **33**, 2143–2146.

38 W. Yuan, Y. Zeng, Y.-Y. Tan, J.-H. Zhou, W.-J. Xu, W.-X. Zhang and X.-M. Chen, *Chem. Commun.*, 2019, **55**, 8983–8986.

39 C. Shi, J. J. Ma, J. Y. Jiang, M. M. Hua, Q. Xu, H. Yu, Y. Zhang and H. Y. Ye, *J. Am. Chem. Soc.*, 2020, **142**, 9634–9641.

40 K. Mencel, V. Kinzhybalo, R. Jakubas, J. K. Zareba, P. Szklarz, P. Durlak, M. Drozd and A. Piecha-Bisiorek, *Chem. Mater.*, 2021, **33**, 8591–8601.

41 M. Wojciechowska, A. Gagor, A. Piecha-Bisiorek, R. Jakubas, A. Cizman, J. K. Zareba, M. Nyk, P. Zielinski, W. Medycki and A. Bil, *Chem. Mater.*, 2018, **30**, 4597–4608.

42 P. Szklarz, A. Gagor, R. Jakubas, P. Zielinski, A. Piecha-Bisiorek, J. Cichos, M. Karbowiak, G. Bator and A. Cizman, *J. Mater. Chem. C*, 2019, **7**, 3003–3014.

43 P. Szklarz, R. Jakubas, W. Medycki, A. Gagor, J. Cichos, M. Karbowiak and G. Bator, *Dalton Trans.*, 2022, **51**, 1850–1860.

44 H.-Y. Shen, L. He, P.-P. Shi and Q. Ye, *J. Mater. Chem. C*, 2021, **9**, 4338–4343.

45 H. Peng, Q. Liu, Y. Liu, Y. Lu and W. Liao, *Chin. Chem. Lett.*, 2023, **34**, 107980.

46 Q. Liu, H. Peng, J.-C. Qi, Y.-Z. Lu, S.-J. Yang and W.-Q. Liao, *Chem. Commun.*, 2023, **59**, 1793–1796.

47 K. Eckhardt, V. Bon, J. Getzschmann, J. Grothe, F. M. Wisser and S. Kaskel, *Chem. Commun.*, 2016, **52**, 3058–3060.

48 R. L. Z. Hoye, R. E. Brandt, A. Osherov, V. Stevanovic, S. D. Stranks, M. W. B. Wilson, H. Kim, A. J. Akey, J. D. Perkins, R. C. Kurchin, J. R. Poindexter, E. N. Wang, M. G. Bawendi, V. Bulovic and T. Buonassisi, *Chem. – Eur. J.*, 2016, **22**, 2605–2610.